17.6 A Sub-40μW 5Mb/s Magnetic Human Body Communication Transceiver Demonstrating Trans-Body Delivery of High-Fidelity Audio to a Wearable In-Ear Headphone

Jiwoong Park, Patrick P. Mercier

University of California, San Diego, La Jolla, CA

Emerging wearable devices such as wireless headphones, smart glasses, and medical monitors require increasingly high-throughput wireless communications at ultra-low-power. Since far-field RF has significant path loss around the human body (e.g., up to 70dB at 2.4GHz), most RF body-area-network (BAN) systems such as Bluetooth Low Energy (BLE) have significant energy-expensive amplification requirements consuming milliwatts of power, and thus do not meet the energy demands of emerging small devices. Popular wireless earbuds, for example, only achieve a battery life of a few hours. Exasperatingly, emerging high-fidelity streaming audio and video content requires higher data rates than what BLE can currently accommodate. Human body communication (HBC) systems, for example ones based on electric fields (eHBC), in theory have lower path loss and can thus potentially offer more efficient links [1-2]. However, measurements from form-factor-accurate prototypes reveal path loss that is still rather large (e.g., 30-to-45dB across 20cm [3]), with unfortunately severe variation with posture and environments that requires energy-expensive compensation. Since the human body is magnetically inert, magnetic HBC (mHBC) systems, illustrated in Fig. 17.6.1, offer much lower path loss (e.g., 5-to-30dB over 1m [4]) without severe variation, and can thus theoretically achieve lower communication energy. However, to date there has not been any mHBC transceiver (TRX) developed to exploit this inherently efficient communication channel, and if there were, the high Q of employed coils would limit data rate of a straightforward approach to <800kb/s.

This paper presents the design of an mHBC TRX that consumes <40μW at a data rate of 5Mb/s, for the lowest energy/bit amongst pragmatic prior art wireless meter-range BAN transceivers. Efficient operation is achieved by: 1) exploiting the intrinsically low path loss between high-Q mHBC coils to reduce TX output power and RX gain/noise requirements; 2) employing an mHBC coil as a high-Q resonant element in an energy-efficient directly-OOK-modulated power oscillator (PO); 3) communicating at a high data rate (5Mb/s) despite the high-Q TX coil, which nominally limits bandwidth to <800kHz, via an all-digital frequency-locked-loop (ADFLL)-based synchronous injection-locked accelerated quenching and kick-start circuit, which also serves to dynamically tune the TX resonant capacitor to maintain center frequency lock between TX and RX while compensating the impedance variation of body-worn coils; and 4) biasing dynamic-threshold MOS (DTMOS) RX amplifiers and envelope detector (ED) in deep subthreshold, all at link-budget-appropriate noise levels.

A block diagram of the proposed mHBC TRX is shown in Fig. 17.6.2. The TRX utilizes a power oscillator to directly generate the 40MHz carrier by using the coil itself as the resonant element in the oscillator [5], as shown in Fig. 17.6.3. However, since the Q of the TX coil can be large (e.g., 50), driving the PO on and off for OOK modulation via the tail transistor cannot be normally accomplished at a data rate faster than 800kb/s. This is one of the reasons why conventional near-field communication (NFC) protocols implementing low-frequency (<13.5MHz) near-field coupling (as opposed to simultaneous near- and far-field coupling at a higher frequency in mHBC [4]) cannot support sufficiently high data rates. Here, to increase data rate, transistors M_{s1} and M_{s2} are deployed to rapidly shunt the inductor current during transmissions of logic '0's. On the other hand, to rapidly kick-start oscillations when transmitting logic '1's, which would normally take more cycles at 40MHz than are available in a 5Mb/s symbol period, injection transistors M_{i1} and M_{i2} are deployed, improving oscillation startup time by 20×. To maximize the effect of injection-locked kick-start, the resonant frequency of the PO, which can change slightly with posture or environmental variation (though not as severely as in eHBC), is precisely set to the same frequency as the crystal-based injection source for synchronous injection via a 4×4 unit-capacitor array that is dynamically tuned via an ADFLL, also shown in Fig. 17.6.3. This also helps to minimize any frequency mismatching between TX and RX. The fast control bit output (2.5Moutput/s) of the ADFLL enables frequency tuning within 10-to-20μs every 1-to-10ms to minimize wait time during calibration.

The RX, shown in Fig. 17.6.3, is designed using a common-source (CS) preamplifier, an active CS envelope detector (ED), a single-ended-to-differential (S-to-D) buffer, and variable gain amplifier (VGA). All RX circuits are biased in subthreshold and utilize DTMOS inputs to improve transconductance or conversion gain by up to 32% iso-current. The ED output drives a S-to-D buffer designed with low-V_t devices to minimize input capacitance to help ensure 2.5MHz bandwidth at the output of the low-current ED; the S-to-D then drives a differential 3b VGA. The VGA output is bit-sliced via a regenerative comparator at the appropriate common-mode voltage thanks to the VGA's common-mode feedback (CMFB) circuit.

The mHBC transceiver is fabricated in 0.12mm^2 of core area in 65nm CMOS. Figure 17.6.4 (top left) shows the output waveform of the TX under worst-case modulation of alternating 1s and 0s at 5Mb/s. Thanks to the accelerated quenching and kick-start circuit, the ASK-like modulation index improves from 15.4% to 84.7% compared to a conventional power oscillator, thereby enabling the desired high data rate in a manner that is compatible with the low-complexity RX. The spectrum of a signal received by an mHBC coil across a 10cm channel is shown in Fig. 17.6.4 (top right). Here, it can be seen that the ADFLL automatically re-tunes the intentionally-mis-tuned PO resonance frequency (~40.4MHz) of TX to the correct carrier frequency (40MHz), while also demonstrating that injection locking further improves total TX output power by 17.4dB while providing the rapid kick-start behavior described above. The inset plot illustrates the frequency-tracking capability of the TX, while validating the fast frequency settling (<10μs) of the ADFLL. BER testing in Fig. 17.6.4 (bottom left) under asynchronous operating conditions with 2× oversampling demonstrates receiver sensitivities of -63.5dBm to -56dBm at data rates from 1.25-to-5Mb/s, respectively, and from -57dBm to -54dBm according to VGA gain setting at 5Mb/s. When operating over a distance of ~1m across a human body, a pair of mHBC TRXs, with -24.8dBm TX output power and the -56dBm RX sensitivity setting, achieved a TX-to-RX latency at 5Mb/s of 388ns with error-free operation, as shown in Fig. 17.6.4 (bottom right).

To demonstrate feasibility of a practical application, two-channel analog audio data was generated by a smartphone and delivered via a two-channel 24b ADC and AES3 encoder to an mHBC TX employing a 2-turn 1mm width coil printed on the outline of 11×5.5cm^2 1oz copper PCB mounted on the smartphone. An mHBC RX, employing a 32mm-diameter coil mounted within an in-ear headphone prototype, wirelessly received data, playing audio data through a speaker via an AES3 decoder and DAC. A block diagram of the test setup is shown in Fig. 17.6.2 (bottom), a photograph of the test in progress is shown in Fig. 17.6.5, and the developed components are shown in Fig. 17.6.6 (top). Here, audio is shown to be delivered from the smartphone case to the headphone prototype across the body with no bit errors and <90μs latency (dominated by the 88μs of latency of the AES3 decoder).

As summarized in Fig. 17.6.6 (bottom), the TX consumes 18.6μW at -24.8dBm of output power, resulting in an efficiency of 3.7pJ/bit at 5Mb/s. At -56dBm sensitivity, the RX consumes 6.3μW for an efficiency of 1.3pJ/bit. When including the power of a 17.2μW crystal oscillator, the TX and RX consume 35.8μW (7.2pJ/bit) and 23.5μW (4.7pJ/bit), respectively, all while reliably covering a ~1.5m BAN. This is the lowest power and most efficient TRX amongst prior-art that reliably communicate over a BAN and that includes the power consumption of frequency synthesis. A die micrograph is shown in Fig. 17.6.7.

Acknowledgement:
This work was supported in part by the National Science Foundation under Grant No. 1751293.

References:

[1] S. Maity, et al., "A 6.3pJ/b 30Mbps -30dB SIR-tolerant Broadband Interference-Robust Human Body Communication Transceiver using Time Domain Signal-Interference Separation," *IEEE CICC*, pp. 1–4, Apr. 2018.
[2] J. Jang, et al., "4-Camera VGA-resolution capsule endoscope with 80Mb/s body-channel communication transceiver and Sub-cm range capsule localization," *ISSCC Dig. Tech. Papers*, pp. 282–283, Feb. 2018.
[3] J. Park, et al., "Channel Modeling of Miniaturized Battery-Powered Capacitive Human Body Communication Systems," *IEEE. Trans. Biomed. Eng.*, vol. 64, no. 2, pp. 452–462, Feb. 2017.
[4] J. Park, et al., "Magnetic Human Body Communication," *IEEE EMBC*, pp. 1841–1844, Aug. 2015.
[5] P. P. Mercier, et al., "A Sub-nW 2.4 GHz Transmitter for Low Data-Rate Sensing Applications," *IEEE J. Solid-State Circuits*, vol. 49, no. 7, pp.1463-1474, July 2014.

 978-1-5386-8531-0/19/$31.00

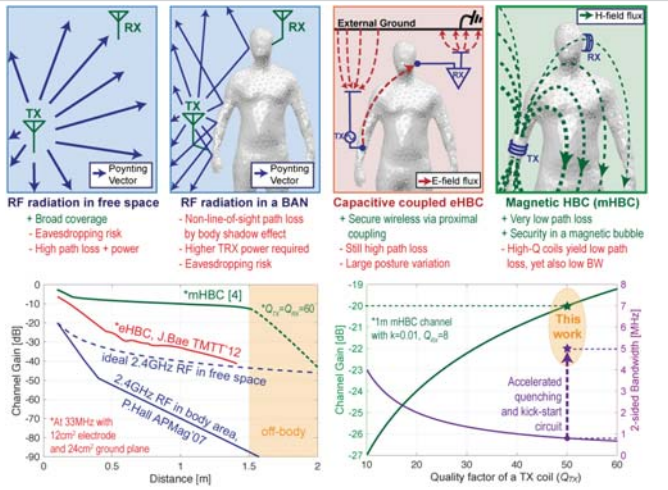

Figure 17.6.1: The path loss of far-field RF, eHBC, and mHBC compared (top and bottom left); increasing the Q of the TX coil decreases path loss, but also nominally decreases bandwidth without the proposed accelerated quenching and kick-start circuit (bottom right).

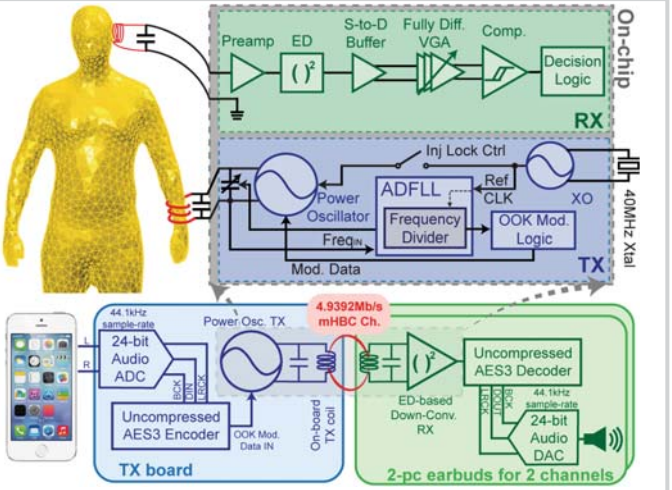

Figure 17.6.2: Block diagram of proposed mHBC transceiver (top); block diagram of the audio streaming demonstration test setup delivering two channels of uncompressed 44.1kHz 24b audio to demonstrate the high-throughput capabilities of the mHBC link (bottom).

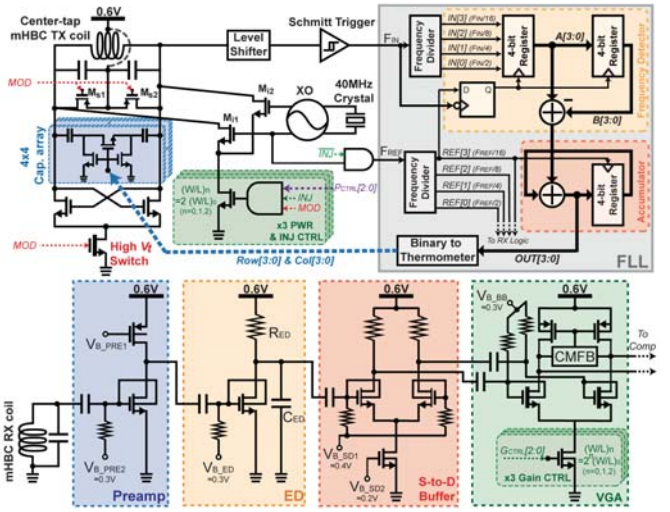

Figure 17.6.3: Schematics of the TX power oscillator and injection locking circuit for the faster-than-Q data-rate modulation (top); the sub-Vt DTMOS envelope-detector based RX (bottom).

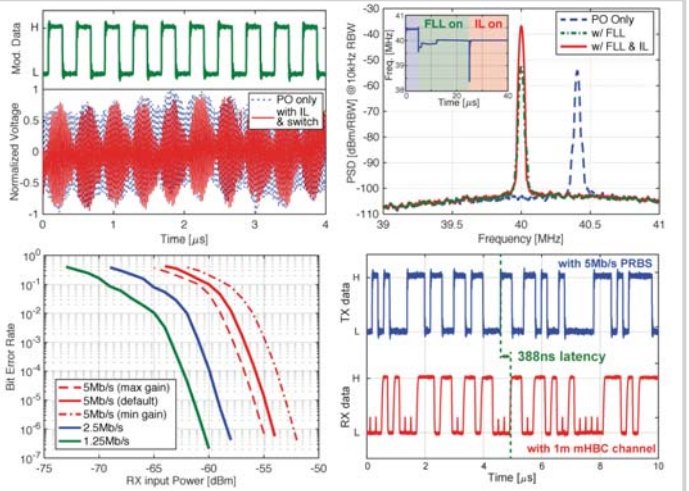

Figure 17.6.4: Measured 5.5× improved worst-case OOK-modulated TX output waveform (top-left), measured spectrum and frequency transient (inset) of dynamic resonance tuning by the ADFLL (top-right), measured RX BER curves (bottom-left), and measured cross-body waveform results (bottom-right).

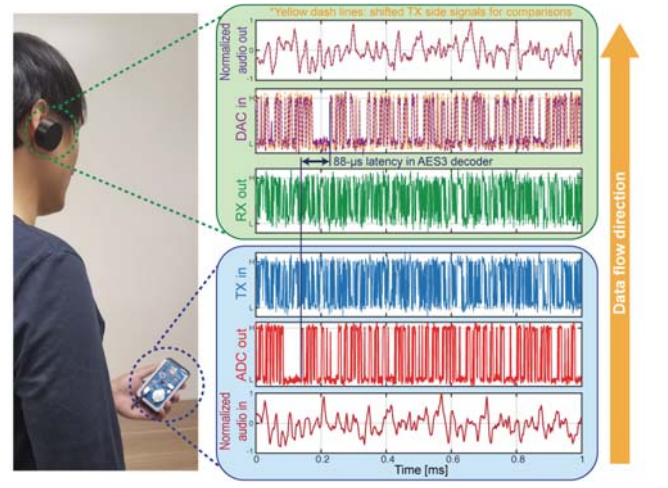

Figure 17.6.5: System demonstration results of high-fidelity audio data streaming (2-channel 24b 44.1kHz audio) via an mHBC link supporting 4.9392Mb/s AES3 format to demonstrate the high-throughput capabilities of the mHBC TRX.

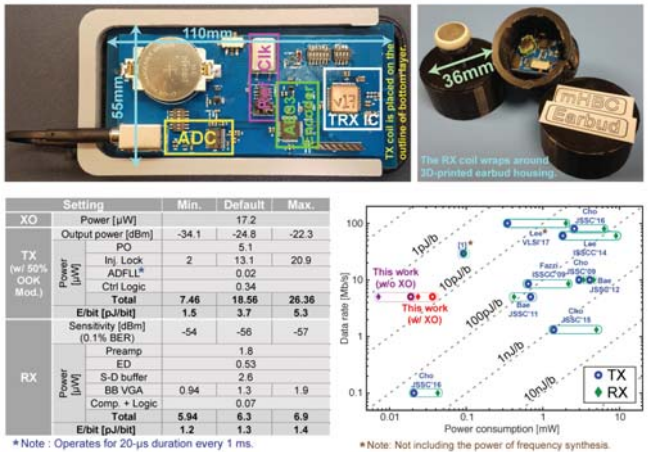

		Setting	Min.	Default	Max.
XO		Power [μW]		17.2	
TX (w/ 50% OOK Mod.)	Power [μW]	Output power [dBm]	-34.1	-24.8	-22.3
		PO		5.1	
		Inj. Lock	2	13.1	20.9
		ADFLL*		0.02	
		Ctrl Logic		0.34	
		Total	7.46	18.56	26.36
		E/bit [pJ/bit]	1.5	3.7	5.3
RX		Sensitivity [dBm] (0.1% BER)	-54	-56	-57
	Power [μW]	Preamp		1.8	
		ED		0.53	
		S-D buffer		2.6	
		BB VGA	0.94	1.3	1.9
		Comp. + Logic		0.07	
		Total	5.94	6.3	6.9
		E/bit [pJ/bit]	1.2	1.3	1.4

*Note : Operates for 20-μs duration every 1 ms.

*Note: Not including the power of frequency synthesis.

Figure 17.6.6: Photograph of the battery-operated audio streaming prototypes: the TX unit fits within a smartphone case (top-left) and the earbud-based RX prototypes were 3D printed for demonstration purposes (top-right); table of specifications (bottom-left), and the state-of-the-art comparison chart (bottom-right).

17

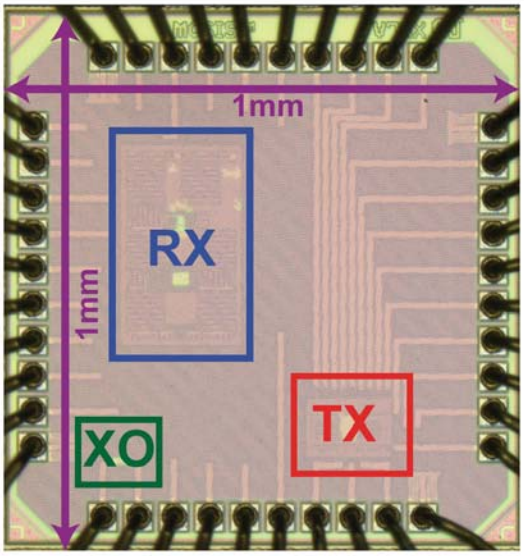

Figure 17.6.7: Die micrograph of the proposed mHBC transceiver.

978-1-5386-8531-0/19/$31.00